Region-shrinking: A hybrid segmentation technique for isolating continuous features, the case of oceanic eddy detection

Qingling Wu[1]

Graduate School of Geography, Clark University, Worcester, MA, USA 01610

qwu@clarku.edu

Correspondence details:

Department of Geography, University College London, London, UK WC1E 6BT

Tel: +44 (0)7526 804954

qingling.wu@ucl.ac.uk

[1] Present address: Department of Geography, University College London, London, UK WC1E 6BT

Abstract

In remote sensing image analysis, limited attention has been devoted to the isolation of fuzzy objects, namely those with inherently indeterminate boundaries, from continuous field data. This study develops a "region-shrinking" segmentation technique tailored specifically to the problem of fuzzy object identification, and applies it to the test case of oceanic eddy detection. The region-shrinking technique employs an evolutionary boundary definition procedure to simultaneously identify segments containing oceanic eddies, and refine the boundaries of these segments to correspond to eddy perimeters. This algorithm combines a Non-Euclidean Voronoi segmentation technique with insights from existing work on eddy detection from an oceanographic perspective, with the goal of improving the detection of eddy features through sea level anomaly imagery. It takes into account multiple criteria (vorticity, size, amplitude, the existence of local sea level extrema, concave or convex shape) to iteratively refine the identification and demarcation of oceanic eddies. The resulting polygons define tightly fitted eddy boundaries, and conform to the key rotational and cross-sectional height profile characteristics used by physical oceanographers to identify eddies.

Keywords: segmentation; object based image analysis; fuzzy objects; oceanic eddies; Okubo-Weiss parameter; sea level anomaly; AVISO

1. **Introduction**

Earth Scientists have long sought to extract climatological phenomena as objects that can be tracked and analyzed. One phenomenon that has received a great deal of attention in this respect is that of mesoscale oceanic eddies. The appearance, transformation, propagation and disappearance of eddies can be identified by human researchers. However, progress has only recently begun to be made in the automation of these identification procedures, limiting the ability of researchers to simultaneously identify, track and analyze the thousands of eddies churning across of the ocean's surface at any given moment. While methods such as the Okubo-Weiss Parameter have recently shown some success as automated eddy detection algorithms (Okubo, 1970; Weiss, 1991; Isern-Fontanet et al., 2003; Chelton et al., 2007; Hanson & Thomas, 2008), these have well-documented limitations hindering their ability to distinguish true eddies from ambient vorticity (Chaigneau et al., 2008; Chelton et al., 2011; Williams et al., 2011). This has sparked interest in the application of polygon-based identification procedures to eddy identification in the past few years (Nencioli et al., 2010; Chelton et al., 2011). This paper introduces an object-based image analysis (OBIA) method for extracting oceanic eddies through the examination of Okubo-Weiss Parameter values and sea-surface height anomalies (SSHA), which incorporates the power of the former as an indicator of eddy vorticity, while using the latter to reduce the prevalence of false positives usually associated with Okubo-Weiss detection. The proposed method has three steps. It first scans for local extreme SSHA pixels. Secondly, it designates these extreme pixels as "seeds" in a Voronoi-inspired segmentation method that uses a non-Euclidean cost-distance allocation technique (Wu & Eastman, under review) to divide the sea surface

58 map into eddy candidate polygons. Thirdly, a region-shrinking style of curve evolution
59 technique is used simultaneously to identify true eddies, and define a tightly fitted
60 boundary for each of these.

61 ## 2. Mesoscale Eddies

62 ### 2.1. Definition and Significance of Mesoscale Oceanic Eddies

63 Oceanic eddies are anomalous volumes of homogeneous ocean water that spin in circular
64 patterns. A very common phenomenon, they trap water from warm or cold ocean currents
65 in their centers, and carry this into areas with a different ambient water temperature
66 (Colling, 2001; Garrison, 2007), often traveling long distances while maintaining their
67 integrity. Oceanic eddies, particularly mesoscale eddies, are believed to have major
68 impacts on phenomena ranging from global ocean current transportation (including the
69 thermohaline circulation and the Antarctic Circumpolar Current), heat and salt transport,
70 carbon flux (i.e. impacts on the uptake and release of dissolved gases), oceanic biology
71 and the fishing industry, and coastal management (Bindoff et al., 2007). For these reasons,
72 mesoscale eddies are of great interest to both biological and physical oceanographers
73 (Perkins, 2007).

74 Eddies are generated from flow instability, predominantly the baroclinic
75 instability of boundary currents and density fronts (Williams & Follows, 2003). Their
76 formation creates regions of strongly contrasting ocean temperature, altimetry, and
77 biological productivity, producing visible and distinct—albeit temporary—boundaries on
78 the ocean surface. Owing to the Rossby radius of deformation (the maximum radius a
79 disturbance can spread as a result of the Coriolis force) in the open ocean, mesoscale
80 eddies range from tens to a few hundred kilometers in diameter (Garrison, 2007;

Robinson, 2010). Changes in sea surface altimetry, temperature or chlorophyll concentration at these scales can be detected through remotely sensed imagery, and an increasing number of researchers have attempted to utilize remote sensing data to identify and track eddies (Isern-Fontanet et al., 2003; Waugh et al., 2006; Chelton et al., 2007; Doglioli et al., 2007; Henson & Thomas, 2008; Fu et al., 2010; Chelton et al., 2011).

2.2. Current studies on identifying mesoscale eddies

2.2.1. Physical parameter based: Okubo-Weiss, Winding Angle, and Wavelet

With the increasing availability of high resolution Maps of Sea Level Anomalies (MSLA) products (e.g. from TOPEX/Poseidon and AVISO), many researchers have developed techniques for extracting oceanic eddies from sea surface height (SSH) data. Until 2008, the Okubo-Weiss Parameter, *W*, was commonly accepted as a standard method for extracting oceanic eddies from MSLA derived velocity fields (Isern-Fontanet et al., 2003; 2006; Chelton et al., 2007; Henson & Thomas, 2008). Sea surface height anomaly (*h*) is measured through radar altimetry , with its first order derivatives in turn used to generate eastward and northward geostrophic velocity anomalies: $u = \frac{-g}{f}\frac{\partial h}{\partial y}$ and $v = \frac{g}{f}\frac{\partial h}{\partial x}$ at location (*x*, *y*), where *g* is the gravitational acceleration and *f* is the Coriolis parameter. Using the eastward and northward velocity (*u* and *v*) components, the Okubo-Weiss Parameter method calculates surface vorticity ($\omega = \frac{\partial \mathrm{v}}{\partial \mathrm{x}} - \frac{\partial \mathrm{u}}{\partial \mathrm{y}}$), normal strain ($\mathrm{s_n} = \frac{\partial \mathrm{u}}{\partial \mathrm{x}} - \frac{\partial \mathrm{v}}{\partial \mathrm{y}}$) and shear strain ($\mathrm{s_s} = \frac{\partial \mathrm{v}}{\partial \mathrm{x}} + \frac{\partial \mathrm{u}}{\partial \mathrm{y}}$), with the Okubo-Weiss parameter itself equaling $\mathrm{W} = \mathrm{s_n}^2 + \mathrm{s_s}^2 - \omega^2$ at each pixel. It then separates velocity fields into vorticity-dominated ($\mathrm{W} < 0$) and strain-dominated ($\mathrm{W} > 0$) regions, with highly vorticity-dominated regions

being designated as eddies (Isern-Fontanet et al., 2003; Chelton et al., 2007; Hansen & Thomas, 2008).

While showing substantial power as a tool for identifying regions of elevated oceanic vorticity, the Okubo-Weiss Parameter method has a number of well-documented limitations as an eddy detection technique (Nencioli et al., 2010; Chelton et al., 2011; Williams et al., 2011). Firstly, it lacks a "universal threshold" for defining high-vorticity pixels. While many studies (e.g. Pasquero et al., 2001; Isern-Fontanet et al., 2006; Hansen & Thomas, 2008) have used -0.2 standard deviations of the W parameter as a threshold for defining high vorticity regions, such a fixed cut-off value does not necessarily produce the most satisfactory results across different regions (Nencioli et al., 2010; Chelton et al., 2011). Lowering or increasing this threshold tends to produce either a loss of sensitivity to small eddy signals, or false positives in eddy areal demarcation. The problem of false-positives is particularly widespread, with the Okubo-Weiss method generally being unable to distinguish fully between eddies and other features exhibiting local vorticity such as stream meanders or simply small-scale high-vorticity noise. The Okubo-Weiss parameter is also highly sensitive to noise in SSHA fields, which is inherently amplified in the calculation of second-order derivatives of SSHA (Chelton et al., 2011). Alternative physical parameter-based eddy identification algorithms, such as the Winding Angle method (Sandarjoen et al., 2000; Chaigneau et al., 2008) and 2-D Wavelet method (Doglioli et al., 2007), have also been developed in parallel with Okubo-Weiss. These other methods, however, have their own weaknesses and limitations, including a lack of computational efficiency, and a dependence on velocity signals which, similar to Okubo-Weiss, contain noise that is often amplified by the analysis (Nenlicio et

126 al., 2010; Chelton et al., 2011; Faghmous et al., 2012). Moreover, "misregistration"
127 between the SSH and velocity fields can be substantial (Chelton et al., 2011), with
128 velocity-based methods tending to produce tail-like or other non-circular shapes in eddy
129 output images as a result.

130 **2.2.2. Flow direction (*u* and *v*) based**

131 Nencioli et al. (2010) developed a vector geometry-based algorithm to detect oceanic
132 eddies, and applied it to 1 km resolution model-generated data from the Regional Oceanic
133 Modeling System (ROMS). Williams et al. (2011) used a similar method to extract eddies
134 from Parallel Ocean Program model data generated by Los Alamos National Laboratory
135 with a grid resolution of approximately 0.1°. Although these algorithms perform well
136 when applied to 1 km or 0.1° resolution simulated data, the widely used 0.25° resolution
137 of available real-world empirical data (specifically AVISO) is insufficient to support
138 these algorithms, with higher resolutions being required for the accurate computation of
139 flow rotations key to the classification of eddies. These resolution requirements are
140 particularly demanding for the detection of smaller eddies (see Constraint IV of
141 Nencioli's algorithm). Recent research has begun to explore the possibility of addressing
142 this limitation through the spatial interpolation of remotely sensed image data into a
143 resolution of 1/6° by 1/6° (Liu et al. 2012).

144 **2.2.3. Contour-based**

145 In 2011, Chelton et al. published a SSHA contour-based method (CH11 hereafter) of
146 eddy extraction, departing from previous research (Chelton et al., 2007) utilizing the
147 traditional pixel-based Okubo-Weiss Parameter based method. The new method proposed
148 by these researchers does not require a global threshold value for either the velocity or

SSHA fields. Rather, it starts with iterative binarization of the SSHA map for all sea surface heights between -100 to +100 centimeter at one centimeter intervals. For the identification of cyclonic (Northern hemisphere cold core) eddies, true values are assigned to pixels with SSHA below each threshold value, while false values are assigned to pixels with SSHA above the threshold. The opposite algorithm is applied for the detection of anticyclonic (Northern hemisphere warm core) eddies. Using this method, closed contour polygons can be drawn around each SSH anomaly, with the assumption being that these contour lines approximately correspond to streamlines surrounding an eddy. Following this step, a series of detection criteria are applied for each SSHA threshold to classify the closed contour polygons into eddies and non-eddies. These detection criteria include polygon size, amplitude, the existence of local SSHA maxima/minima, and the distance between any two points within the closed contour.

This method has proven to be superior to Okubo-Weiss Parameter in terms of its ability to avoid noise and false positive eddy detections (Chelton et al., 2011; Styles et al. 2012). It still has certain limitations, however, notably a difficulty differentiating between multiple connected eddies with the same polarity (Chelton et al., 2011), and a rootedness in computationally inefficient repeated binarization calculations and N-nearest neighbor searches (Faghmous et al., 2012).

A small number of studies (Styles et al., 2012; Faghmous et al., 2012) have sought to build upon and improve the methods used in Chelton et al. (2011), attempting to reduce the computational demands of this approach by eliminating the need for exhaustive N-nearest neighbor searches of point pair distances within eddy candidates. Proposed replacements for the N-nearest neighbor search include the restriction of eddy

polygons to convex hull shapes (Styles et al., 2012) and the classification of eddies based on information from previous and subsequent time slices (Faghmous et al., 2012). Although these studies were able to break apart "larger than normal" eddy candidates into multiple distinct eddies, iterative image binarization remains essential to the capture of SSH anomalies in these newer methods, which as a result have remained relatively computationally inefficient.

2.2.4. Trend: Beyond pixel-based identification

In summary, it is generally accepted that pixel-based methods of eddy extraction have inherent limitations (Doglioli et al., 2007; Nencioli et al., 2010; Chelton et al., 2011), with recent research thus shifting towards the extraction of eddies as whole/continuous objects delineated by closed contour boundaries, These contour-based approaches, which strive to identify eddies at a higher level of abstraction, are still in their infancy from an object-based image analysis (OBIA) perspective. Here, a segmentation-based method is proposed for identifying eddies from SSHA and velocity fields. This new object-based image analysis technique is not only aimed at improving existing techniques in the context of the specific task of eddy identification, but is rooted in more abstract and flexible conceptual foundations which make it of greater relevance to the problem of fuzzy object identification and analysis in general (Jacquez et al., 2000; Yuan, 2001; Cova & Goodchild, 2002; Goodchild et al., 2007).

OBIA and segmentation techniques classify images not only based on spectral information, but also spatial homogeneity and contiguity. In the past, OBIA has been generally used to extract geographic features such as land cover zones (Walter, 2004; Benz et al., 2004; Blaschke, 2009; Dey et al., 2010), which have relatively distinct

physical boundaries. In contrast, existing/mainstream segmentation techniques have only shown a limited ability to isolate amorphously-bounded features such as oceanic eddies (Wu & Eastman, under review). As such, the method proposed here not only constitutes an advance in the area of automated eddy detection, but a more basic methodological advance with broader applications.

3. Data

Archiving, Validation, and Interpretation of Satellite Oceanographic Data (AVISO)—which is generated from a combination of data from Topex/Poseidon, Jason-1 & 2 and Envisat –has been a commonly used sea surface height dataset (Ducet et al., 2000; Pascual et al., 2006; AVISO: http://www.aviso.oceanobs.com). Many existing studies aimed at eddy extraction have used AVISO as their primary data source (Isern-Fontanet et al., 2006; Chelton et al., 2007; Chaigneau et al., 2008; Henson & Thomas, 2008; Chelton et al., 2011). AVISO altimetry data is gridded into maps of sea level anomalies (MSLA) every seven days at a spatial resolution of 1/4°x1/4°. Here, one time slice of the AVISO MSLA data of the Reference Series from the first week of 2009 is employed to demonstrate the new technique.

4. Methodology

For the purposes of analysis, an eddy is defined here as a dome- or bowl-shaped structure rotating around a SSHA extreme at its center. A stylized (Northern Hemisphere) cyclonic eddy has a concave shape, with a local minimum SSHA value at its center; conversely, an anticyclonic eddy has a convex shape, with a local maximum SSHA value at the center. In image analysis terms, a cyclonic eddy can be intuitively conceptualized as a concave basin that sucks-in and spins water around a core of minimum SSHA in

relation to outlying pixels within this basin. Conversely, an anticyclonic eddy can be seen as a convex mound surrounding a local maximum sea surface height core at the rotational axis. Existing studies (Chaigneau et al., 2008; Chelton et al., 2011) extract eddies based on the assumption that these are SSH anomalies on an otherwise flat ocean surface. In contrast, the method proposed here assumes that the ocean's surface is in practice entirely subdivided into bulges and basins, each of which constitutes a potential eddy candidate. These bulges and basins can be thought of forming a tessellation of regions which are more strongly influenced by one potential eddy core than by any other.

As many (Sadarjoen and Post 2000; Isern-Fontanet et al. 2003; Doglioli et al. 2007; Nencioli et al. 2010; Chelton et al. 2011) have noted, there is no general agreement among researchers regarding the definition of eddy boundaries. For the purposes of an initial demonstration of the general methodology, this paper sidesteps these disagreements, and instead proposes an algorithm which seeks to achieve accurate eddy detection by initially targeting eddy candidate cores. It then confirms or disconfirms the status of each eddy candidate on the basis of whether the core's surrounding region meets multiple loosely defined detection criteria. The emphasis in this procedure is on an evaluation of eddy candidacy through the testing of whole object characteristics.

With this in mind, the proposed eddy detection technique consists of three stages. Firstly, the SSHA imagery is scanned to locate all seed, i.e. local SSHA minima and maxima, each of which is designated as a candidate of eddy core. Here, a pixel in the SSHA image is identifies as a *seed* when its value is higher or lower than all of its eight neighboring pixels, with seeds thus corresponding to all *local extrema* in the image.

240 Next, a cost-distance based *Non-Euclidean Voronoi (NEV)* segmentation
241 technique (Wu & Eastman, under review) is used to exhaustively divide the SSHA image
242 into "bulge" and "basin" eddy candidate polygons centered on one and only one seed
243 each. For every non-seed pixel, the cost-distance is calculated as the sum of slope along
244 the path to its closest seed, where the slope surface is standardized into a one-to-ten scale.
245 This cost-distance measure is based on the assumption that eddies will tend to be
246 bounded by relatively steeply-sloping SSHA gradients (i.e. high velocity streamlines).
247 Every non-seed pixel is grouped into its closest seed in terms of cumulative slope,
248 meaning each seed aggregates a group of pixels that form a polygon surrounding the seed
249 itself. This method is similar to the traditional Voronoi polygon (Okabe et al., 1992), but
250 uses a form of non-Euclidean distance measurement. Thus, each polygon here is named a
251 Non-Euclidean Voronoi (NEV) segment. When the seed is a local SSHA maximum, a
252 polygon is designated as a warm core eddy candidate; conversely, where the seed is a
253 local SSHA minimum, a polygon is designated as a cold core eddy candidate.
254 Finally, these eddy candidate polygons are subjected to an iterative region-
255 shrinking procedure which simultaneously determines whether they are in fact true eddies,
256 and defines a tightly fitted boundary for each of these (as opposed to the loosely-fitted
257 initial NEV boundaries). This procedure shrinks the outermost layer of pixels (i.e.
258 boundary) of each eddy candidate towards its core, one pixel width at a time. For each of
259 these iterations, a checklist of criteria (described below) is applied to the pixels within the
260 boundary of each eddy candidate polygon. If all criteria are met at a particular iteration,
261 this candidate is classified as an eddy, with boundaries corresponding to the boundary
262 established at this iteration. Otherwise, the algorithm continues to shrink the perimeter of

eddy candidate polygons towards their centers (i.e. seeds), until each is either classified as an eddy, or is reduced in size to a minimum specified size (8 pixels) at which point it is discarded as a candidate. Lastly, each confirmed eddy polygon is circularized based on its diameter, defined by the shorter of either latitudinal or longitudinal spans.

Figure 1 shows a flowchart detailing the region-shrinking algorithm (R-S hereafter). The seed identification procedure is an essential step in the common region-growing segmentation method. The second step, the NEV segmentation procedure is a non-Euclidean variant of a Voronoi Diagram. It uses a cumulative cost-distance to local extreme in SSHA seeds to partition MSLA image into regions dominated by eddy candidates (Wu & Eastman, under review; Grey boxes in Figure 1). Lastly, the region-shrinking method can be categorized as a type of curve evolution technique that recursively refines segmentation boundaries. Hence, the new method can be seen as a hybrid segmentation technique combining aspects of the three types of segmentation techniques. The role of the NEV segmentation technique here is to divide the sea surface into neighborhoods each dominated by an individual eddy candidate. Then, the region-shrinking segmentation technique refines each neighborhood boundary until each is classified as either an eddy or a non-eddy region.

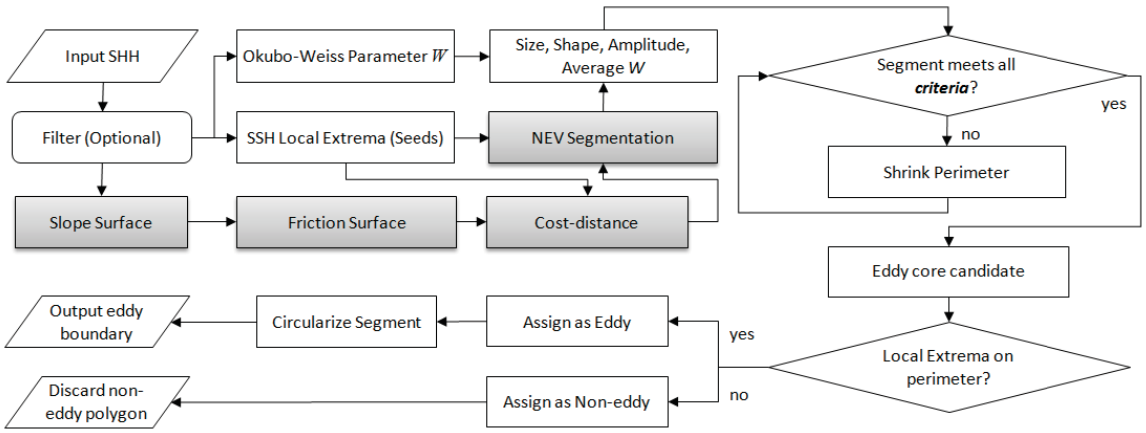

Figure 1. Flowchart of R-S: region-shrinking eddy detection method with NEV segmentation (grey boxes) incorporated.

For the purposes of an initial demonstration of the general methodology proposed here, the eddy detection criteria applied while shrinking the polygons are as follow:

a) *Average W for all pixels within an eddy boundary < -0.025:*

Based on the rotating nature of oceanic eddies, it is necessary to confirm that a candidate eddy is on average more vorticity-dominated than strain-dominated. Hence, the first eddy detection criterion is that an eddy polygon have an average Okubo-Weiss Parameter of no more than -0.025 ($\overline{W} < -0.025$). In previous studies using the Okubo-Weiss Parameter for purposes of eddy identification (Pasquero et al., 2001; Isern-Fontanet et al., 2006; Chelton et al., 2007; Hanson & Thomas, 2008), concerns have often been raised that the global *W* threshold used was either too low or too high, resulting in either a general prevalence of false positive or false negative eddy detections. As the eddy detection algorithm proposed here has the advantage of cross-checking eddy classifications using multiple criteria, it was decided to use a very undemanding average *W* threshold (-0.025, as compared to -0.2 used by most studies), to separate vorticity-dominated regions from strain-dominated regions for all the pixels within an eddy boundary. This allows the average *W* criterion itself to retain small-scale potential eddies,

299 relying on the other identification criteria to eliminate the numerous false positives
300 among eddy candidates at this scale. The fact that *W* is only evaluated in an average sense
301 across the whole eddy polygon also bypasses problems stemming from the noisy nature
302 of derived vorticity fields which are associated with pixel-based Okubo-Weiss
303 approaches.

304 ***b)*** *Amplitude > 1cm:*

305 The second criterion for eddy classification is the requirement that the SSHA at
306 an eddy seed (i.e. center) diverge (in either the positive or negative direction) by at least 1
307 cm from the average SSHA at the eddy perimeter. This difference in SSHA is calculated
308 as: $\text{Amp} = |h_{seed} - h_0|$, where h_{seed} is the SSHA at seed and $h_0$is the average SSHA
309 value around the perimeter of an eddy candidate. The imposition of a 1 cm minimum
310 threshold on this amplitude difference in this eddy identification algorithm follows
311 Chelton et al. (2011), who argue that this is an effective compromise between excessively
312 high thresholds that produce an abundance of false negatives, and excessively low
313 thresholds that result in noisy, "ameba-shaped" eddy boundaries.

314 ***c)*** *Size >= 8 pixels*

315 The preprocessing of AVISO Reference Series attenuates features with radius
316 smaller than 0.4° (Chelton et al., 2011), necessitating the inclusion of a minimum size
317 criterion in the eddy identification algorithm. Chelton et al. (2011) limit the minimum
318 size of eddies to 8 pixels, which is roughly equivalent to a 0.4° radius given the
319 resolution of the AVISO Reference Series. In contrast, Styles et al. (2012) apply a
320 slightly different minimum requirement of 9 pixels for the purposes of their shape-based
321 identification algorithm. Both the 8- and 9-pixel eddy minimum eddy-size criteria were

322 tested, and very similar results were produced - Among the 0.5% extra eddies produced
323 with the 8-pixel limitation, most are small eddies whose core is in close vicinity to
324 another eddy candidate. As nearly all of these small-scale candidates appear to be true
325 eddies, it was decided to adopt an 8-pixel minimum size threshold.

326 ***d)*** *Concave or convex shape:*

327 A (Northern Hemisphere) anticyclonic eddy is expected to have a convex cross-
328 section, with maximum SSHA at its center, while a cyclonic eddy is expected to present
329 the opposite vertical profile. Styles et al. (2012) improved CH11by testing for a
330 "convexity ratio parameter", calculated as the ratio of a feature's area to its convex hull
331 area (in which a value of 1 indicates perfectly consistent convexity). This technique,
332 however, has the disadvantage of relying on a rather subjective concavity index threshold
333 definition (specifically 0.85). With this in mind, the method proposed here employs a
334 convexity algorithm that bypasses this type of subjective threshold requirement. This
335 algorithm calculates the average SSHA of all pixels within the candidate polygon at an
336 incremental given distance (in pixel widths) away from the potential eddy center. For an
337 anticyclonic eddy, the average SSHA at any given distance from the eddy center must
338 decrease as this distance increases; conversely, for a cyclonic eddy, the average SSHA
339 must increase as distance to the eddy center increases.

340 In summation, the above criteria diverge from existing eddy identification
341 algorithms in that they are based on the simultaneous analysis of Okubo-Weiss Parameter
342 values and sea surface height anomalies. Solely examining the Okubo-Weiss Parameter
343 (Isern-Fontanet et al., 2003; 2006; Chelton et al., 2007) guarantees the extraction of high
344 vorticity fields (Williams et al., 2010; Chelton et al., 2011); however, not all of the high

vorticity fields identified will be eddies. Meanwhile, contour-based eddy extraction methods (Chelton et al., 2011; Styles et al., 2012) are able to identify prominent sea surface height anomalies with convex or concave shapes; the SSH anomalies thereby identified, however, may or may not exhibit the rotation inherently associated with true eddies. Keeping in mind these pitfalls associated with each of these "pure" approaches, the hybrid approach proposed here ensures that each eddy has both a minimum specified level of both active rotation and vertical prominence.

5. Results

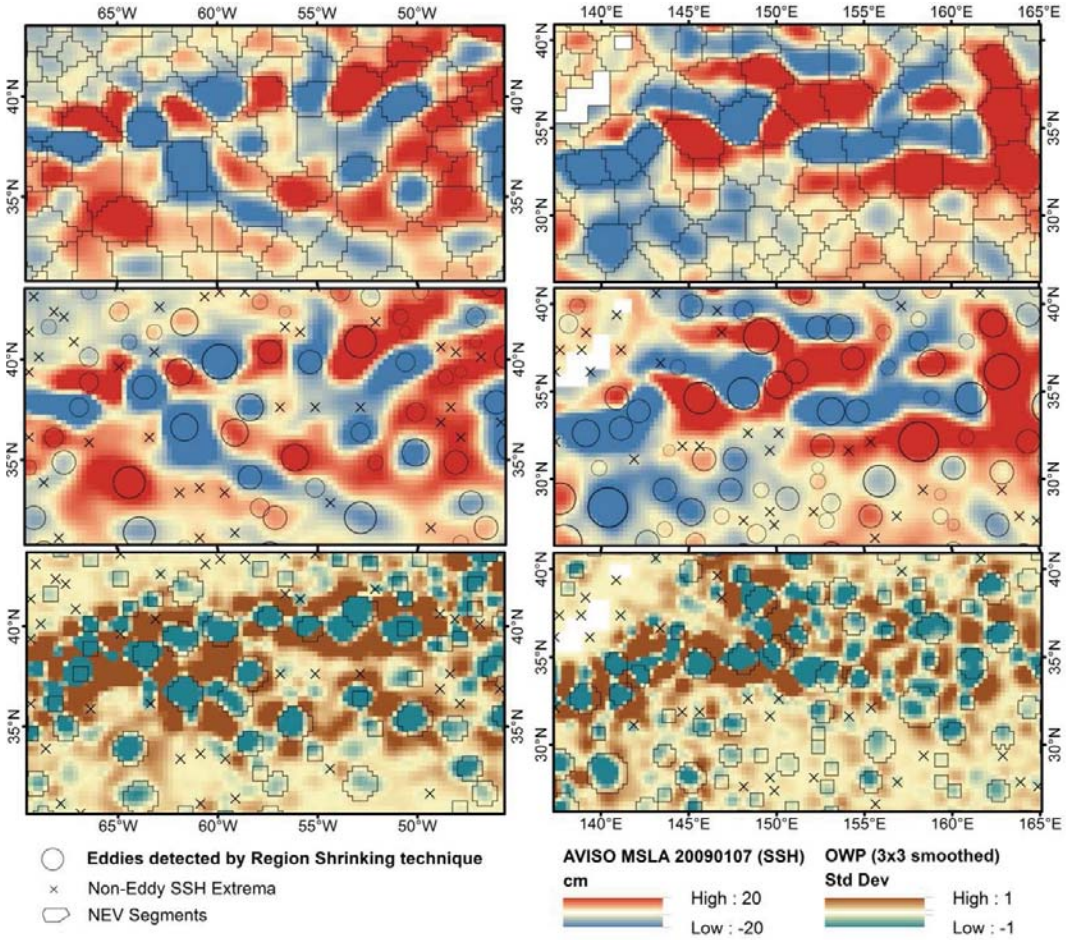

Figure 2. Eddies produced by R-S method superimposed on SSHA and Okubo-Weiss Parameters, 1st week of 2009 (Left: along the Gulf Stream; Right: the Northeastern Pacific). Polylines in top two images represent regional boundaries produced by NEV segmentation technique. Hollow circles (○) in the middle and bottom figures represent eddies detected by R-S (boundaries smoothed in middle figure for aesthetic purposes). SSHA Local Extrema discarded as eddy cores are marked with crosses (×).

Figure 2 illustrates two sample views of the NEV segmentation results of eddy candidate polygons (top two figures), and the refined eddy polygons identified by the R-S technique (circles in the middle and bottom figures). In the single time slice of the first week of 2009, under the criteria mentioned in the methodology section, 5233 out of 11764 SSHA local extrema were classified as eddy cores (see Figure 2 for zoomed sample views). Among these 5233 eddies, 2646are cyclonic and 2587 are anticyclonic. All eddies identified exhibit some degree of internal rotation as tested by average Okubo-Weiss Parameter; in contrast, many regions with high Okubo-Weiss Parameter values were not designated as eddies. These regions often correspond to *false positive* eddies detected by pure Okubo-Weiss based methods. Some examples can be seen in patches of blue in Figure 2 (bottom) where no eddy was identified. On the other hand, CH11 is known to be unable to differentiate between connected eddies. An example of three connected eddies can be seen in Figures 2 (also see white boxes in Figure 4) at roughly 33N° and 141E°. These three connected eddies, immediately off the Japanese coast, form a SSH anomaly region that CH11 classified as a single eddy. However, the SSHA extrema scanning step at the beginning of the proposed procedure was immediately able to identify three individual eddy core candidates, which an inspection of the Okubo-Weiss Parameter and other criteria confirmed as true eddies in the subsequent region-shrinking algorithm.

CH11 found 1350 cyclonic and 1309 anticyclonic eddies in the same time slice, or approximately half of the number of eddies detected using the proposed R-S method here. CH11 however only presented eddies that lasted at least 4 weeks. As such, a direct comparison of results requires that eddies persisting less than 4 weeks be removed from the R-S results, as shown in Figures 3 and 4.

382 Figure 3 illustrates the progression of eddy cores from December 17th 2008 to
383 January 7th 2009 (eddies lasting at least 4 weeks ending on January 7th 2009) in the
384 Northeast Pacific. The movement of individual eddies can be easily seen. If an eddy core
385 at time *t* falls into an eddy boundary of a sequential *t+1*, this eddy is considered to have
386 survived for at least two weeks; if the core of such eddy at *t+1* falls into a boundary at
387 *t+2*, then the same eddy is considered to have lasted for at least three weeks. The same
388 procedure was applied for three weeks before and after the sample time slice (*t-3, t-2, …,*
389 *t+3*) to locate all eddies that have survived for at least 4 weeks including January 7th 2009.

390 Among all eddies that survived the first week of 2009, 3196 were found to have
391 lasted at least 4 weeks including the first week of 2009 (Figure 5; referred as 4+ week
392 eddies hereafter), as compared to 2659 eddies detected by CH11. That is, R-S detects 20%
393 more eddies than CH11 when the 4-week restriction is applied (Table 1). Table 1 shows
394 nearly 60% of the 4+ week eddies produced by R-S fall directly within CH11 eddy
395 polygons, and 88% of 4+ week R-S eddy cores are no more than 5 pixels away from any
396 CH11 eddy polygons, and vice versa. This comparison shows a general level of
397 agreement between the two techniques. The disagreements, on the other hand, are
398 principally due to 1) eddies missed by CH11 approach due to the method's weakness at
399 separating connected eddies; 2) false-positive eddies lacking vorticity detected by the
400 CH11 on the basis of SSHA; and 3) the fact that a number of 4+ week eddies from the
401 CH11 were only identified by R-S as lasting 3 weeks or less, due to low vorticity or
402 amplitudes towards the end or beginning of their life cycles.

403 Figure 4 shows eddies lasting at least 4 weeks, with cores marked by crosses,
404 alongside 4+ week eddies identified by CH11, with cores marked by black dots. Two out

405 of the three connected eddies at roughly 33ºN 141ºE were identified by R-S as lasting for
406 4+ weeks (Figure 4). Similarly, another three pairs of connected eddies, at roughly 30 ºN
407 147ºE, 34ºN 154ºE and 38 ºN 153ºE respectively, were successfully differentiated by R-S,
408 whereas CH11 detected them as individual connected eddies.

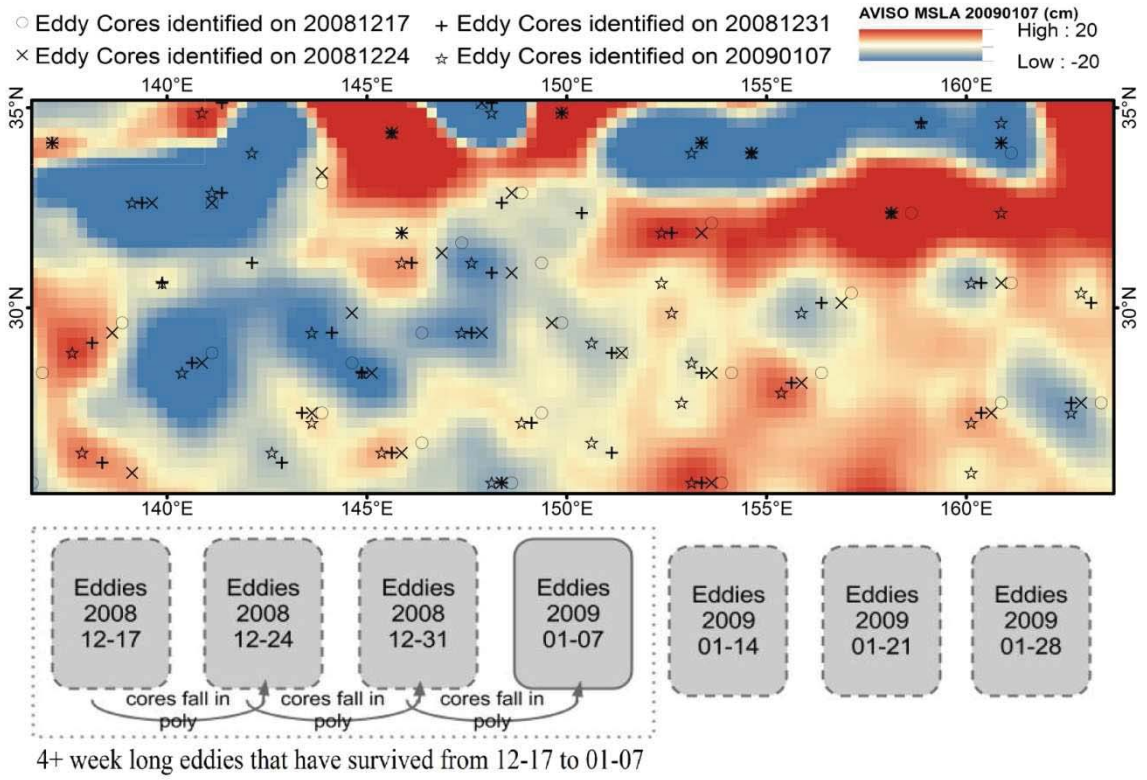

409

410 Figure 3. (Top) Eddy cores identified over four continuous weeks. (Bottom) Eddy tracking scheme: If any
411 eddy core from the previous time slice can be located within an eddy boundary at a particular time, then
412 such an eddy is regarded as having survived for two continuous weeks. Likewise, eddies that have lasted at
413 least 4 weeks can be identified across the study period.

414 Table 1. Comparison between the numbers of eddies found by CH11 and R-S.

	CH11	R-S
Number of eddies found in time slice	Unknown (3000+)	5233
Number of eddies lasting at least 4 weeks	2659	3196
Number of eddy cores falling within eddy boundaries identified by other method	1599 (60% of 4-week eddies identified)	1855 (58% of 4-week eddies identified)
Number of eddy cores falling into buffer zones (0.5º, 2 pixel distance) surrounding eddy boundaries identified by other method	2034 (76% of 4-week eddies identified)	2299 (72% of 4-week eddies identified)
Number of eddy cores falling into buffer zones (1.25º, 5 pixel distance) surrounding eddy boundaries identified by other method	2328 (88% of 4-week eddies identified)	2827 (88% of 4-week eddies identified)

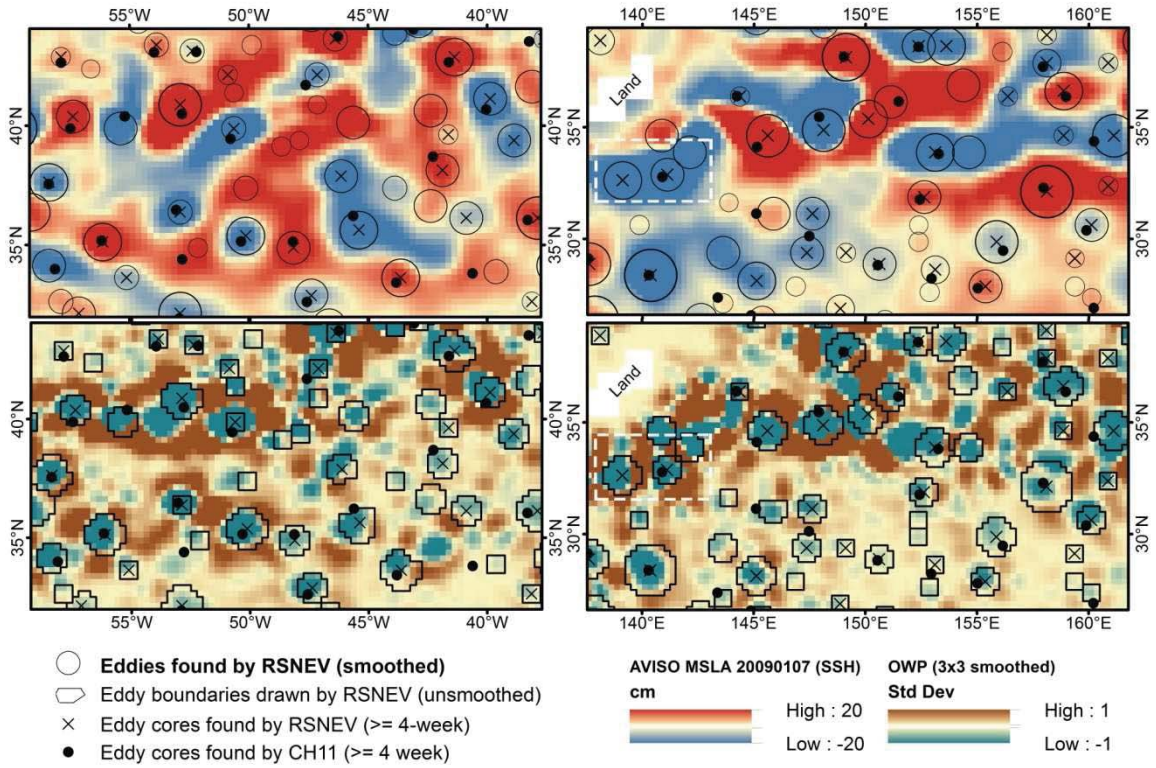

Figure 4. North Atlantic eddies superimposed on SSHA (top) and Okubo-Weiss Parameters (bottom). Eddy cores identified by CH11 (Data exported by Duke MGET) are shown as black dots (●); Eddy cores identified as lasting at least 4 weeks by R-S are marked with crosses (x). Eddy boundaries defined by R-S method are drawn as circles (O).

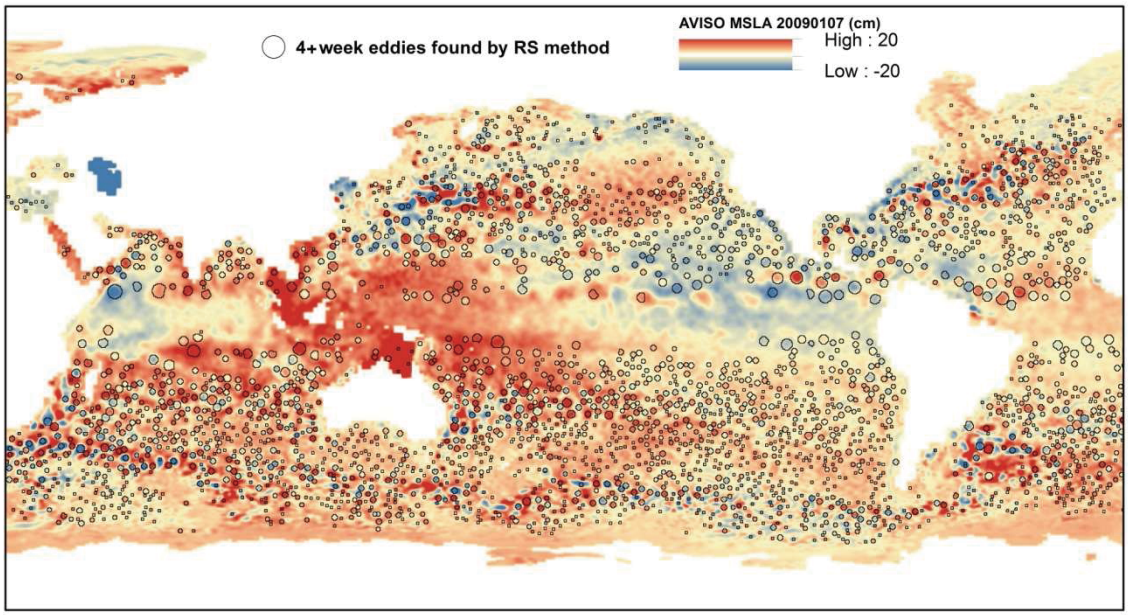

Figure 5. Map of global eddies (lifespan >= 4 weeks) detected by R-S during the first week of 2009. Among the 3196 eddies found, 1643 are cyclonic (yellow/blue to blue) and 1553 are anticyclonic eddies (yellow/red to red).

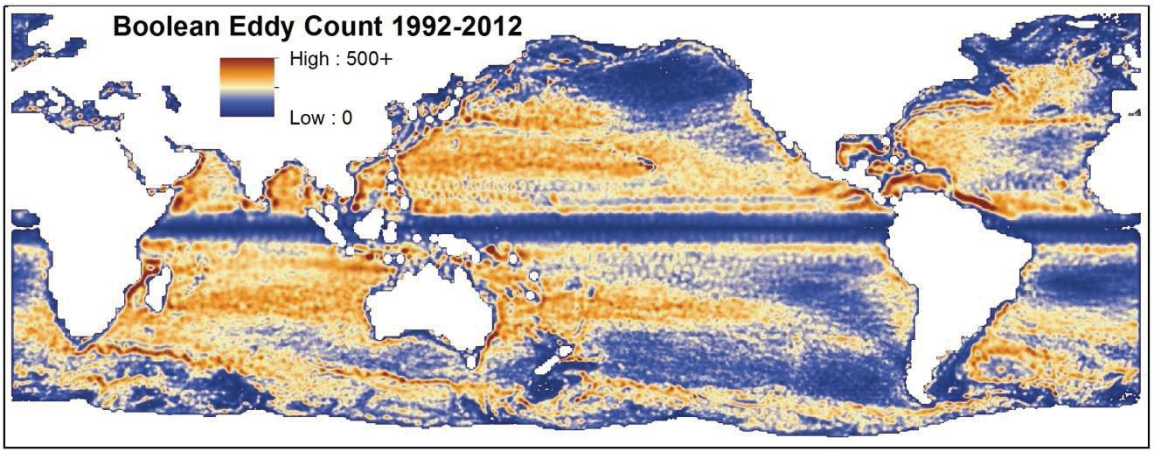

Figure 6. Map of global eddy count from October 1992 to July 2012. Pixel values represent the total number of weeks that any eddy has existed over that pixel.

Figure 6 shows a global eddy count map produced by the R-S technique, over the period October 1992 to July 2012. Pixel values present the total numbers of weeks that any eddy has existed over that location. It clearly shows several "eddy highways" (brown areas) in which eddies to be present more often than other areas of the ocean. Areas along the Gulf Stream, Kuroshio Extension, Eastern Australian Current, North Brazil Current, Agulhas Current and Mozambique Channel exhibit the highest frequencies of eddies, as do many continental margins.

6. Discussion

While there is general agreement between the eddy results produced by this study and the results produced by CH11 (Chelton et al., 2011; Duke MGET), this proposed R-S technique finds 20% more eddies than CH11, and offers several improvements over existing eddy detection methods. Firstly, the new method does not require iterative binarization of SSHA imagery. Rather, a single scan of the image is sufficient to identify all potential eddy centers. Secondly, unlike Okubo-Weiss Parameter (Isern-Fontanet et al., 2003) based eddy detection, this new method requires no precise adjustment of criteria for different regions of the world's oceans. Rather, the reliance on multiple loose-

444 threshold criteria means that common parameters can be used globally. Thirdly, the basin
445 allocation procedure, NEV segmentation, used in this new method creates a clear
446 delineation between closely spaced neighboring eddies, including those of the same
447 polarity. The ambiguity in defining, or inability to detect such boundaries altogether in
448 the case of multi-core eddies, has been identified as a widespread problem in other eddy
449 identification procedures (Chelton et al., 2011; Style et al., 2012). Fourthly, it ensures
450 that all detected eddies demonstrate both rotational characteristics and a concave or
451 convex shape.

452 Moreover, the multi-criteria eddy identification algorithm employed in the region-
453 shrinking procedure is object-based, insofar as eddy status is confirmed or disconfirmed
454 through an analysis of the combined characteristics of all pixels lying within an eddy
455 candidate polygon at each iteration. It emphasizes the accurate identification of eddies
456 through the identification of seeds, and the examination of the overall characteristics of
457 each objects. The detection results are thus insensitive to small differences in eddy
458 boundary location, which improves the robustness of the procedure given the lack of
459 general agreement on eddy boundary definition.

460 It should be noted that the region-shrinking algorithm could be easily adapted to
461 iteratively refine eddy boundaries on the basis of more complex criteria (e.g. contour
462 lines, velocity) in order to more accurately represent eddy shape. Hypothetically, these
463 small but plausible changes in shape could be made to define eddy boundaries, with little
464 effect on the number of eddies being detected. Taken as a whole, these varied plausible
465 results could be considered to comprise a fuzzy boundary set, defining a zone of greater
466 or lesser pixel eddy membership probability around any given eddy core.

Building upon a number of existing eddy detection methods (Isern-Fontanet et al., 2003; Isern-Fontanet et al., 2006; Chelton et al., 2007; Chaigneau et al., 2008; Nencioli et al., 2010; Chelton et al., 2011; Styles et al., 2012) and object-based segmentation techniques (Benz et al., 2004; Jones et al., 2005; Wu & Eastman, under review), the region-shrinking segmentation technique demonstrated here is clearly capable of identifying oceanic eddies. However, it has a few limitations. The Okubo-Weiss parameter used in this analysis was calculated based on eastward and northward velocity (u and v) values obtained from the AVISO database, which become unreliable in the equatorial region (~5°N to ~5°S) due to very low Coriolis effect strength. The identification of eddies could therefore be compromised between ~5°N and ~5°S (Chaigneau et al., 2008; AVISO). In addition, although not the focus of this paper, the 4-week tracking method applied to the extraction of long-lasting eddies in this study is still relatively primitive. Further research needs to be carried out to enhance the temporal tracking technique.

7. Summary and Conclusion

The primary goal of this study was to develop a region-shrinking segmentation technique tailored specifically to the problem of identifying continuous features, and apply it to the demonstration case of oceanic eddy detection. In summary, the method proposed here first scans for all local extreme SSHA pixels, and uses them as "seeds" in a cost-distance Voronoi segmentation algorithm to divide the sea surface map into eddy candidate polygons. Lastly, a region-shrinking style of curve evolution technique is used simultaneously to identify true eddies, and define a tightly fitted boundary for each of these. The region-shrinking technique employs an evolutionary boundary definition

procedure to draw tightly fitted eddy boundaries. The use of multiple eddy selection criteria enables the refined identification of eddy polygons exhibiting combinations of key rotational characteristic and gradual changes in height across their profiles.

More broadly, the region-shrinking segmentation technique, like other OBIA techniques, is intended to bridge raster and vector-based methods of analysis, and provide outputs that can directly be fed into secondary study including statistical analysis, object tracking over time, change detection analysis, and the like. This proposed method and the case study presented demonstrate that OBIA, as a simulation of human perceptual powers, has the ability to extract a broad range of "objects", including not only those with clearly defined boundaries but also objects with indeterminate or fuzzy boundaries (Smith, 2001; Cova & Goodchild, 2002; Cheng et al., 2001) such as oceanic eddies. Ultimately, the goal of the region-shrinking segmentation technique demonstrated is not simply to improve on existing eddy detection techniques. Rather, it also hopes to open new directions in the application of evolutionary OBIA techniques to fuzzy geographical object identification in general. Indeed, the iterative shrinkage of segment boundaries is a dynamic evolutionary procedure that can be applied to many other applications including cell delineation in medical imagery, and the identification of hilltops and pollution plumes. More broadly, it promises to contribute to the progression of computerized image analysis from the mere presentation and processing of data, to the perception and analysis of higher-order features.

References

AVISO Data available from http://www.aviso.oceanobs.com/.

Bindoff, N. L., J. Willebrand, V. Artale, C. A, J. Gregory, S. Gulev, K. Hanawa, C. L. Quéré, S. Levitus, Y. Nojiri, C. K. Shum, L. D. Talley & A. Unnikrishnan (2007). Observations: Oceanic Climate Change and Sea Level. In S. Solomon, D. Qin, M. Manning, Z. Chen, M.

Marquis, K.B. Averyt, M. Tignor & H.L. Miller (Eds.), *Contribution of Working Group I to the Fourth Assessment Report of the Intergovernmental Panel on Climate Change 2007* (pp. 385-429). Cambridge, United Kingdom and New York, NY, USA.: Cambridge University Press, (Chapter 5).

Benz, U. C., Hofmann, P., Willhauck, G., Lingenfelder, I., & Heynen, M. (2004). Multi-resolution, object-oriented fuzzy analysis of remote sensing data for GIS-ready information. *ISPRS Journal of Photogrammetry and Remote Sensing, 58*(3-4), 239-258.

Blaschke, T. (2010). Object based image analysis for remote sensing. ISPRS Journal of Photogrammetry and Remote Sensing, **65**(1): 2-16.

Chaigneau, A., A. Gizolme & C. Grados (2008). Mesoscale eddies off Peru in altimeter records: Identification algorithms and eddy spatio-temporal patterns. Progress In Oceanography, **79**(2-4): 106-119.

Chelton, D. B., M. G. Schlax, R. M. Samelson & R. A. de Szoeke (2007). Global observations of large oceanic eddies. Geophysical Research Letters, **34**(15): L15606.

Chelton, D. B., M. G. Schlax & R. M. Samelson (2011). Global observations of nonlinear mesoscale eddies. Progress In Oceanography, **91**(2): 167-216.

Cheng, T., M. Molenaar & H. Lin (2001). Formalizing fuzzy objects from uncertain classification results. International Journal of Geographical Information Science, **15**(1): 27-42.

Colling, A. (2001). Ocean Circulation. Oxford, UK, Butterworth-Heinemann.

Cova, T. J. & M. F. Goodchild (2002). Extending geographical representation to include fields of spatial objects. International Journal of Geographical Information Science, **16**(6): 509-532.

Dey, V., Y. Zhang & M. Zhong (2010). A review on image segmentation techniques with remote sensing perspective. ISPRS TC VII Symposium - 100 Years ISPRS, Vienna, Austria, IAPRS.

Doglioli, A. M., B. Blanke, S. Speich & G. Lapeyre (2007). Tracking coherent structures in a regional ocean model with wavelet analysis: Application to Cape Basin eddies. Journal of Geophysical Research, **112**(C5): C05043.

Ducet, N., P. Y. Le Traon & G. Reverdin (2000). Global high-resolution mapping of ocean circulation from TOPEX/Poseidon and ERS-1 and -2. Journal of Geophysical Research, **105**(C8): 19477-19498.

Duke Marine Geospatial Ecology Tools (MGET) http://mgel.env.duke.edu/mget/

Faghmous, J., Y. Chamber, F. Vikebø, S. Boriah, S. Liess, M. d. S. Mesquita & V. Kumar (2012). A novel and scalable spatio-temporal technique for ocean eddy monitoring. Twenty-Sixth Conference on Artificial Intelligence (AAAI-12), 2012.

Garrison, T. S. (2007). Oceanography: An Invitation to Marine Science. Belmont, CA, Thomson.

Goodchild, M. F., Yuan, M., & Cova, T. J. (2007). Towards a general theory of geographic representation in GIS. *International Journal of Geographical Information Science, 21*(3), 239-260

Henson, S. A. & A. C. Thomas (2008). A census of oceanic anticyclonic eddies in the Gulf of Alaska. *Deep-Sea Research I*, **55**: 163-176.

Isern-Fontanet, J., E. García-Ladona & J. Font (2003). Identification of marine eddies from altimetric maps. *Journal of Atmospheric and Oceanic Technology*, **20**(5): 772-778.

Jacquez, G. M., Maruca, S., & Fortin, M. J. (2000). From fields to objects: A review of geographic boundary analysis. *Journal of Geographical Systems, 2*(3), 221-241

Jones, T., Carpenter, A., & Golland, P. (2005). Voronoi-Based Segmentation of Cells on Image Manifolds. In Y. Liu, T. Jiang & C. Zhang (Eds.), *Computer Vision for Biomedical Image Applications* (Vol. 3765, pp. 535-543): Springer Berlin Heidelberg.

Liu, Y., Dong, C., Guan, Y., Chen, D., McWilliams, J., & Nencioli, F. (2012). Eddy analysis in the subtropical zonal band of the North Pacific Ocean. *Deep Sea Research Part I: Oceanographic Research Papers, 68*(0), 54-67.